Journal of Catalysis **204,** 420–427 (2001)
doi:10.1006/jcat.2001.3391, available online at http://www.idealibrary.com on IDEAL®

Noble Metal Segregation and Cluster Size of $Pt/Rh/CeO_2/\gamma\text{-}Al_2O_3$ Automotive Three-Way Catalysts Studied with Low-Energy Ion Scattering

Wim P. A. Jansen,*,† Jan M. A. Harmsen,†,‡ Arnoud W. Denier v.d. Gon,† Jozef H. B. J. Hoebink,†,‡ Jaap C. Schouten,†,‡ and Hidde H. Brongersma*,†,[1]

*Calipso LEIS Expertise Centre, P.O. Box 513, 5600 MB Eindhoven, The Netherlands; and †Schuit Institute of Catalysis and ‡Laboratory of Chemical Reactor Engineering, Eindhoven University of Technology, P.O. Box 513, 5600 MB Eindhoven, The Netherlands

Received May 14, 2001; revised August 2, 2001; accepted August 14, 2001; published online October 25, 2001

A method for determining the average cluster size of supported catalysts using low-energy ion scattering (LEIS) data is presented. The method is particularly suitable for determining the average cluster size of atomically dispersed metals and can be used for clusters as large as 10 nm. For $Pt/\gamma\text{-}Al_2O_3$ quantitative agreement is shown between the average cluster size as determined with LEIS and that determined with transmission electron microscopy (TEM). In the case of three-way catalysts, classic methods for determining the cluster size, such as TEM or CO chemisorption, often fail or produce ambiguous results because of the presence of ceria. Therefore, LEIS has been applied to determine the average noble metal cluster size of a commercial three-way catalyst. Moreover, it is shown by LEIS that the three-way catalyst contains mixed Pt/Rh clusters, which are strongly enriched in surface Pt after reduction.

Key Words: **automotive catalysis; cluster size; nanocluster; segregation; LEIS; ISS.**

1. INTRODUCTION

Three-way catalysts are widely used in new cars for the simultaneous oxidation of hydrocarbons and carbon monoxide as well as reduction of nitric oxide from the exhaust of the engine. This is possible because of the precise lambda controller, which keeps the composition of the exhaust gas near stoichiometric. In reality, the composition will oscillate with a frequency of about 1 Hz around the stoichiometric point, thus inducing transient behavior upon the monolithic converter. After a cold-start of a car, the temperature of the catalytic surface causes the kinetics of the oxidation and reduction reactions to be too slow to obtain the required conversion.

A detailed transient kinetic model based on elementary reaction steps would allow optimization of the currently used catalysts as well as the control system (1). A model-based controller could be used for optimizing conversions based on model calculations. Research at Eindhoven University of Technology (The Netherlands) aims at construction of such a model (2).

For kinetic modeling, information about the noble metal dispersion is a primary requirement. Also for catalyst optimization and for research on catalyst aging, information about the average cluster size is important. Classic methods of obtaining this type of information, such as CO chemisorption, may fail or give ambiguous results for ceria-containing catalysts, where huge CO storage capacities have been found compared with similar catalysts without ceria (3–5). Holmgren *et al.* (6) used a temperature of 195 K to suppress the influence of ceria. At this temperature the CO uptake on ceria was strongly suppressed but not completely hindered. Apart from the influence of ceria, chemisorption may fail because of anomalous average metal coordination numbers at highly dispersed surfaces (7). The latter is explained by an increased probe-molecule-to-metal stoichiometry for metal atoms situated at the corners and edges of small metal clusters. Moreover, the possibility of dissociative CO adsorption on small Pt particles (1–3 nm) deposited on alumina has been reported (8, 9). Transmission electron microscopy (TEM) or high-resolution electron microscopy (HREM) is difficult to perform on ceria-containing catalysts due to the low contrast between the noble metal and the ceria (10).

This paper investigates the possibility of using low-energy ion scattering (LEIS) to determine the average noble metal cluster size of a commercial $Pt/Rh/CeO_2/\gamma\text{-}Al_2O_3$ catalyst. Because LEIS selectively probes the outermost atomic layer, only the surface of a cluster is visible. Therefore, the noble metal LEIS yield depends not only on the total metal loading and the specific surface area but also on the fraction of the atoms in a cluster that are accessible to LEIS. This fraction depends on the cluster size. Therefore, the average cluster size of a catalyst can be determined with LEIS if the total metal loading and the specific

[1] To whom correspondence should be addressed. Fax: 31 40 2453587. E-mail: H.H.Brongersma@tue.nl.

0021-9517/01 $35.00

surface area are known. The method has been verified by using a Pt/γ-Al_2O_3 catalyst to compare the calculated average cluster size from LEIS signals with the average cluster size as determined by TEM. After verification, LEIS has been applied to determine the average cluster size of the ceria-containing commercial three-way catalyst. Moreover, LEIS has been used to solve the question whether the three-way catalyst contains separate Pt and Rh clusters or mixed Pt/Rh clusters.

2. EXPERIMENTAL

2.1. Catalyst Pretreatment

The Pt/γ-Al_2O_3, Rh/γ-Al_2O_3, and Pt/Rh/γ-Al_2O_3 catalysts and a commercial Pt/Rh/CeO_2/γ-Al_2O_3 catalyst, as used for coating monoliths, were provided by d**mc**^{2} A.G. (Hanau, Germany) as powders with a mean particle diameter of 12 μm. The powders were pressed, crushed, and sieved to obtain fractions with pellet diameters between 0.11 and 0.15 mm. To enhance isothermicity during kinetic measurements, the catalysts were diluted with inert α-Al_2O_3 (0.15–0.21 mm) in the ratio of 1.5 g of α-Al_2O_3/1 g of catalyst material. To enable reproducible kinetic experiments, the following pretreatment was carried out for all catalysts. The catalyst was heated to 773 K in a steady flow of He. Then the catalyst was oxidized for 1 h under a stream containing 25 vol% oxygen. Next the catalyst was kept under flowing He for 30 min to purge reversibly adsorbed oxygen, followed by reduction in a He stream containing 5 vol% H_2 at 773 K for 2 h. Finally, the catalyst was allowed to cool down to reaction temperature under a He stream.

Prior to LEIS analysis, all powder samples were compacted into pellets at 300 MPa. Recently, we showed that compaction at 300 MPa does not influence the surface composition (11). LEIS selectively probes the outermost atomic layer, and hence surface contaminants would obscure the intrinsic composition and must be removed before analysis of the intrinsic composition is possible. To clean the samples an atomic oxygen beam was used. The use of atomic oxygen permits very effective cleaning at low temperatures (ca. 310 K) (12). After the oxidative cleaning process, the samples were reduced at 573 K in 20 kPa H_2 flowing at 2.6 mmol/min for 10 min. At 573 K the noble metals were reduced and sintering did not occur (12).

After evacuation, hydrogen from the reduction treatment remains on the surface. This remaining hydrogen can be selectively removed by very light sputtering, since the sputter rate for hydrogen is usually 10 to 50 times higher than that for other elements (13). From LEIS measurements as a function of ion dose, it appeared that hydrogen was removed from a three-way catalyst at a He dose of 2×10^{15} ions/cm^2 (12). Between a He dose of 2×10^{15} and 10×10^{15} ions/cm^2 the surface composition and the elemental LEIS yields of the catalyst remained unchanged. In this study 3-keV Ne ions have been used to allow separation of Pt and Ce in the catalyst carrier. The sputter rate of Ne is typically 10 times higher than that for He. Therefore, all presented measurements were carried out using Ne doses between 0.2×10^{15} and 1×10^{15} ions/cm^2.

2.2. Low-Energy Ion Scattering

In LEIS (also known as ion scattering spectroscopy or ISS) experiments, low-energy noble gas ions are scattered by atoms in the exposed surface. According to the laws of conservation of energy and momentum, the energy spectrum of the backscattered ions is equivalent to the mass spectrum of the target atoms. The information depth of LEIS is limited to one atomic layer because of the high neutralization probability of the noble gas ions.

Earlier studies on Pt/Rh alloys have shown that the LEIS sensitivities for Pt and Rh can be successfully calibrated using pure Pt and Rh reference samples (14, 15). Moreover, these studies showed that after prolonged sputtering with either 2 or 3 keV Ne, the bulk ratio of the Pt/Rh alloy is obtained.

A cluster may be damaged due to the dissipated energy of an impinging ion. Molecular dynamics have shown, however, that the backscattered ion is already on its way back to the detector before this happens (16). LEIS analysis will therefore not be influenced as long as the same spot is not probed more than once. Hence, LEIS measurements must be carried out with a low ion dose. All LEIS measurements were performed in the UHV Calipso LEIS setup. This setup, which was developed at the Eindhoven University of Technology, is equipped with a sensitive double-toroidal analyzer and a large position-sensitive detector. These allow measurement of a large part of the energy spectrum simultaneously (17). The very high sensitivity enables one measure the noble metal concentrations down to some 10 ppm of a monolayer with a relatively low dose. To spread the dose over a larger area, the primary ion beam is rastered over an area of 2×2 mm^2 during measurements. In the Calipso LEIS setup the primary ion beam is directed perpendicular toward the target, and ions scattered over 145° with respect to the incoming beam are detected. During the experiments, the catalyst samples were prevented from charging by flooding with low-energy electrons from all directions.

2.3. Transmission Electron Microscopy

TEM has been performed using a Philips CM 30 T electron microscope with a LaB_6 filament as the electron source. The TEM was operated at 300 kV. Samples were mounted on a microgrid carbon polymer supported on a copper grid by placing a few droplets of a suspension of ground sample in ethanol on the grid, followed by drying under ambient conditions.

3. RESULTS

3.1. Transmission Electron Microscopy

Figure 1 shows a TEM micrograph of Pt/γ-Al_2O_3. Throughout the sample many small metal clusters can be observed. The cluster size distribution is homogeneous. Most clusters are about 0.5–3 nm in diameter, with a few clusters up to about 7.5 nm present as well. When TEM is applied to Pt/Rh/CeO_2/γ-Al_2O_3, the metal particles are obscured from proper imaging due to their low contrast with the ceria particles.

3.2. Upper Limit of the Pt Surface Atom Density at the Pt/γ-Al_2O_3 Surface

A first calculation concerns the maximum possible Pt surface atom density that is attained if all platinum in the Pt/γ-Al_2O_3 is monoatomically spread and present in the outermost atomic layer. Using the metal weight fraction and the BET specific surface area (σ) of the Pt/γ-Al_2O_3 as summarized in Table 1, the maximum number of Pt atoms per unit surface area is

$$\text{surface atom density} = \frac{\text{metal weight fraction} \times N_A}{M_{\text{metal}} \times \sigma}, \quad [1]$$

where N_A is Avogadro's number, and M_{metal} is the molar mass of the metal ($M_{Pt} = 195$ g/mol). The number of Pt atoms per unit surface area for monoatomically spread Pt that is selectively present in the outermost atomic layer is thus calculated as 6.4×10^{16} Pt atoms/m^2 catalyst. Using the bulk atomic density of pure Pt (6.58×10^{28} atoms/m^3 (19)), the volume of 6.4×10^{16} Pt atoms equals 9.7×10^{-13} m^3. Assuming the surface atom density of Pt is $(6.58 \times 10^{28})^{2/3} = 1.6 \times 10^{19}$ atoms/m^2, the maximum Pt surface atom density for the Pt/γ-Al_2O_3 is $6.4 \times 10^{16}/1.6 \times 10^{19}$, which equals a coverage of 4.0×10^{-3} ML. A monolayer (ML) here is defined as 1.6×10^{19} atoms/m^2.

3.3. Pt Surface Atom Density at the Pt/γ-Al_2O_3 Surface for Reduced Pt Clusters

Platinum in Pt/γ-Al_2O_3 is not monoatomically spread over the outermost atomic layer, but present in clusters.

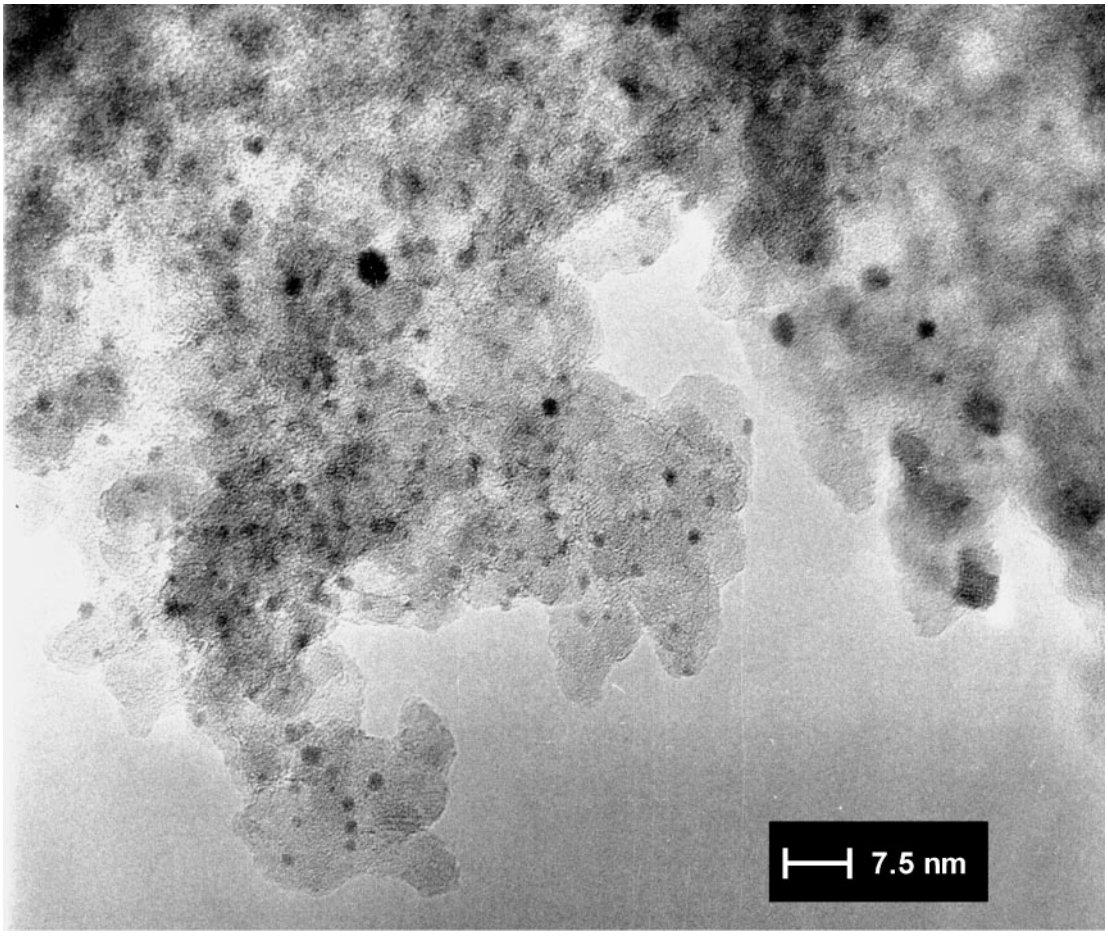

FIG. 1. TEM micrograph of Pt/γ-Al_2O_3. Throughout the sample many small metal clusters can be observed. Most clusters are about 0.5–3 nm, with a few larger clusters present as well.

TABLE 1

Physical Characteristics of the Examined Catalyst

	$Pt/\gamma\text{-}Al_2O_3$	$Rh/\gamma\text{-}Al_2O_3$	$Pt/Rh/\gamma\text{-}Al_2O_3$	$Pt/Rh/CeO_2/\gamma\text{-}Al_2O_3$
Pt g/g catalyst (ICP)[a]	3.98×10^{-3}	—	3.98×10^{-3}	3.98×10^{-3}
Rh g/g catalyst (ICP)[a]	—	7.9×10^{-4}	7.9×10^{-4}	7.9×10^{-4}
σ (m^2/g) (BET)[a]	193	193	193	157
ϑ_{Pt} (ML) (LEIS)	$(1.1 \pm 0.1) \times 10^{-3}$	—	$(0.8 \pm 0.1) \times 10^{-3}$	$(1.0 \pm 0.1) \times 10^{-3}$
Relative ϑ_{Rh} (LEIS)	—	3.2 ± 0.3	1.000	—
Average d (nm) (LEIS)	1.6	—	2.7[b]	2.7
d (nm) (TEM)	0.5–3 few up to 7.5	—	—	—

[a] Inductively coupled plasma (ICP) and BET analysis of the catalyst materials are described in (18).

[b] This value for d is obtained assuming the surface composition of the clusters of the $Pt/Rh/\gamma\text{-}Al_2O_3$ equals that of the $Pt/Rh/CeO_2/\gamma\text{-}Al_2O_3$.

Since the $Pt/\gamma\text{-}Al_2O_3$ has been reduced prior to the LEIS analysis, the Pt atoms are in a metallic state. Metallic Pt atoms will tend to cluster because of their high surface free energy (20–22). TEM pictures of reduced Pt on an oxidic support show spherically shaped Pt clusters (see Fig. 1 and (23)). For molten Pt droplets on an oxidic carrier, the contact angle is approximately 115° (22). Figure 2 shows a schematic of such a cluster with radius r and contact angle α. The volume of clusters with contact angle α equals $c_\alpha \times \pi \times r^3$, where c_α is a geometric factor. Thus for $\alpha = 90°$ (hemisphere) and $\alpha = 180°$ (complete sphere), $c_\alpha = 2/3$ and 4/3, respectively. Figure 3 shows c_α as a function of α. If we define $V_{cluster}$ as the total volume of all clusters on a square-meter catalyst and N as the number of clusters present on 1-m^2 catalyst support, then

$$V_{cluster} = N \times c_\alpha \times \pi \times r^3. \quad [2]$$

As shown in the previous section, $V_{cluster} = 9.7 \times 10^{-13}$ m^3 for the $Pt/\gamma\text{-}Al_2O_3$ catalyst. Only part of the atoms in these clusters will be visible because of shielding by the neighboring surface atoms because the surface is not atomically smooth. V.d. Oetelaar *et al.* (24) showed the effective surface coverage of the spherically shaped clusters as detected by LEIS, A_{vis} as represented in Fig. 2, to be given by

$$A_{vis} = \pi \times r^2. \quad [3]$$

Experimentally it was found that the Pt LEIS yield for the diluted $Pt/\gamma\text{-}Al_2O_3$ was only 0.044 ± 0.004% of that of

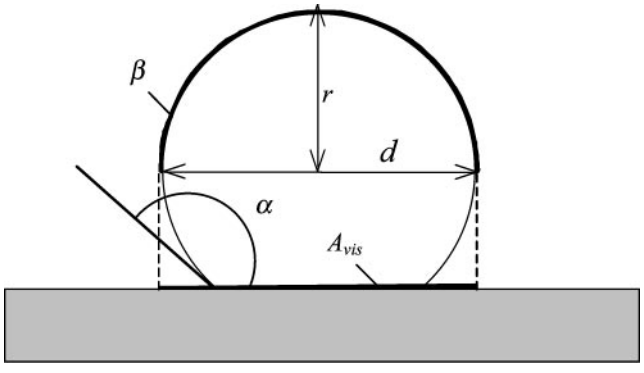

FIG. 2. Schematic illustration of a supported particle with contact angle α, radius, r, and diameter D. Adapted from V.d. Oetelaar *et al.* (24). In LEIS, the surface area β is projected to A_{vis}.

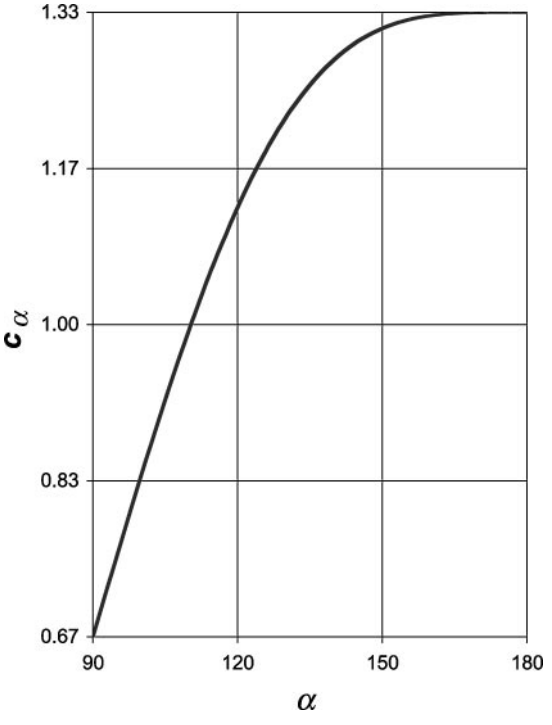

FIG. 3. The geometric factor c_α as a function of the contact angle α. The volume of a spherically shaped cluster equals $c_\alpha \times \pi \times r^3$.

a sputter-cleaned pure polycrystalline Pt sample. If corrections for the dilution of the catalyst with α-Al_2O_3 and for the surface roughness of the compacted powder (11) and the sputter-induced roughness on the Pt reference sample (25) are included, a Pt surface coverage (ϑ) corresponding to $\vartheta = N \times A_{vis} = (1.1 \pm 0.1) \times 10^{-3}$ ML is found for pure Pt/γ-Al_2O_3. Using this value for ϑ, the average cluster radius r of the Pt/γ-Al_2O_3 is given by

$$r = \frac{N \times \pi \times r^3}{N \times \pi \times r^2} = \frac{\left(\frac{1}{c_\alpha}\right) \times \left(\frac{\text{metal weight fraction}}{\sigma \times \rho_{\text{metal}}}\right)}{\vartheta}, \qquad [4]$$

where ρ_{metal} is the volumetric density ($\rho_{Pt} = 21.45 \times 10^6$ g/m^3 (19)). The average cluster diameter (d) of the Pt clusters in Pt/γ-Al_2O_3 as determined from the LEIS measurements is $d = 1.6$ nm. The error margin in d results from both the accuracy of the determination of ϑ and the accuracy of the model assuming ϑ to be equal to $N \times \pi \times r^2$. The error margin in ϑ is 10%, resulting in a 10% error margin for d as well. For the accuracy of the assumption, the error estimation is more difficult; however, its validity is shown in (24).

Another important parameter that can influence the validity of the average particle size as determined with LEIS is the particle size distribution. Let us first consider an example of a Gaussian particle size distribution since this type of distribution occurs frequently (26). Analyzing a Gaussian distribution centered around 3 nm with a full-width half-maximum of 2 nm, an average particle size of 2.7 nm would be found using LEIS. Hence, in the case of a Gaussian particle size distribution LEIS gives a representative value for the average particle size. Evaluating a distribution which is a combination of very small (e.g., 0.4-nm) and larger particles (e.g., 6 nm), LEIS may give an underestimation of the average cluster size. For instance, LEIS would give an average cluster size of only 0.8 nm for a catalyst containing equal amounts of 0.4- and 6-nm clusters. In this case, however, microscopic techniques would have failed as well, since 0.4-nm particles cannot be resolved with either HREM or TEM. Hence, if possible, a combination of microscopic techniques and LEIS may give additional information on the particle size distribution, especially since LEIS probes a statistical average over several square-millimeters of catalyst, whereas microscopic techniques probe only minute areas. Moreover, the accuracy of LEIS increases with increasing dispersion, since LEIS selectively detects atoms in the outermost atomic layer (27). Therefore, very small clusters can be determined with the highest possible accuracy, whereas microscopic methods are limited by a minimum cluster size visibility criterion.

In the case of the Pt/γ-Al_2O_3 catalyst, TEM measurements showed cluster sizes in the range of 0.5–3 nm with a few up to 7.5 nm. Hence, the average cluster size as determined with the LEIS measurements (i.e., 1.6 nm) is well within the range of the TEM measurements. In the case of the Pt/Rh/CeO_2/γ-Al_2O_3 three-way catalyst, TEM is not feasible since the ceria carrier obscures proper imaging of the metal particles. Both Pt/γ-Al_2O_3 and Pt/Rh/CeO_2/γ-Al_2O_3 are synthesized in a similar way. Hence, for the latter a homogeneous particle size distribution, where the average cluster size given by LEIS is accurate, can be expected as well. Moreover, Sections 3.4 and 3.5 will show that the Pt/Rh surface ratio as determined with LEIS can provide additional information on the cluster size of this catalyst.

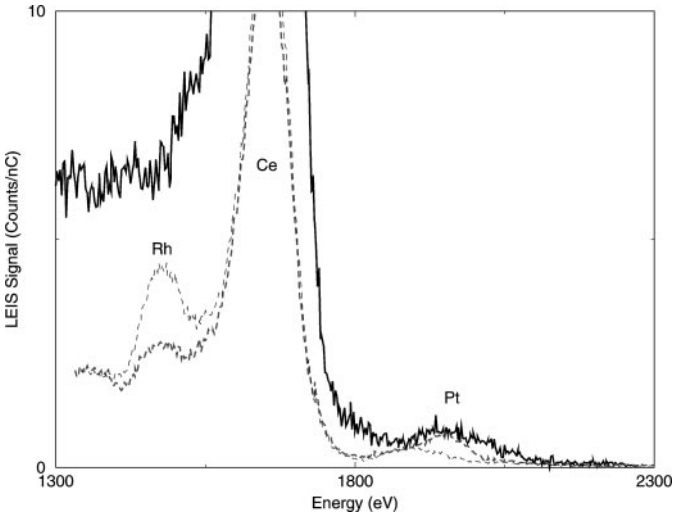

FIG. 4. LEIS spectra of Rh/γ-Al_2O_3 (thin dashed line), Pt/Rh/γ-Al_2O_3 (thick dashed line), and Pt/Rh/CeO_2/γ-Al_2O_3 (solid line) measured with 3 keV Ne^+. The intense Ce peak masks the presence of Rh in the three-way catalyst. The small Ce peaks in Rh/γ-Al_2O_3 and Pt/Rh/γ-Al_2O_3 are due to contamination. All catalysts contained equal Rh wt%.

3.4. LEIS Analysis of Pt/Rh/CeO_2/γ-Al_2O_3

Figure 4 shows LEIS spectra of Rh/γ-Al_2O_3 (thin dashed line), Pt/Rh/γ-Al_2O_3 (thick dashed line), and the Pt/Rh/CeO_2/γ-Al_2O_3 three-way catalyst (thick solid line) measured with 3 keV Ne^+. Apparently, Rh/γ-Al_2O_3 and Pt/Rh/γ-Al_2O_3 are contaminated with Ce (~2 wt%). The Rh LEIS peak is on the low-energy side of the huge Ce peak. The figure shows that the Rh surface coverage in the Pt/Rh/CeO_2/γ-Al_2O_3 catalyst will be indiscernible from the Ce background of the catalyst carrier. To enable the determination of the Rh surface atom density and possible Pt segregation, we have also measured Pt/Rh/γ-Al_2O_3 and Rh/γ-Al_2O_3. The absence of the huge Ce peak allows Rh detection in both Pt/Rh/$\gamma$$Al_2O_3$ and Rh/γ-Al_2O_3 samples. Although all catalysts contain equal Rh wt%, the Rh surface atom density of the Rh/γ-Al_2O_3 is 3.2 ± 0.3 times higher than that of Pt/Rh/γ-Al_2O_3. Hence, if the catalysts contain separate Pt and Rh clusters, the Rh cluster volume in Rh/γ-Al_2O_3 would have to be $(3.2)^{3/2} = 5.7$ times smaller than that in Pt/Rh/γ-Al_2O_3. Since Rh/γ-Al_2O_3 and

Pt/Rh/γ-Al_2O_3 have been similarly prepared, a huge difference in cluster volume is not likely. The observed difference in the Rh surface atom density can be explained, however, by mixed Pt/Rh clusters, where part of the Rh in Pt/Rh/γ-Al_2O_3 is covered with Pt. This is very likely since Pt segregation has been shown for single crystalline Pt/Rh alloys of various compositions after annealing in vacuum or reduction at elevated temperatures (14, 15, 28). Hence, the catalyst does not contain many separate Pt and Rh clusters, but mainly mixed Pt/Rh clusters. A Pt/Pd/Rh/CeO_2/Al_2O_3 automotive catalyst, manufactured by W. R. Grace, contained mixed noble metal clusters as well (26). Only bi- and trimetallic particles were observed in that particular study using analytical electron microscopy, which was possible because this catalyst contained only 2% Ce.

Experimentally it was found that the Pt LEIS yield for the diluted Pt/Rh/CeO_2/γ-Al_2O_3 catalyst was only 0.040 ± 0.004% of that of a sputter-cleaned pure polycrystalline Pt sample. If corrections for the dilution with α-Al_2O_3, the surface roughness of the compacted powder (11), and the sputter-induced roughness on the Pt reference sample (25) are applied, a Pt coverage corresponding to $\vartheta = (1.0 \pm 0.1) \times 10^{-3}$ ML is found for the outermost atomic layer of the Pt/Rh/CeO_2/γ-Al_2O_3 catalyst.

In the next section the surface Pt to Rh ratio of the catalyst will be calculated from the bulk composition using thermodynamics and LEIS data previously obtained on a single crystalline $Pt_{0.25}Rh_{0.75}$. Moreover, the calculated Rh depletion will be compared to the measured depletion on the Pt/Rh/γ-Al_2O_3.

3.5. *Influence of Segregation in Pt/Rh/CeO_2/Al_2O_3 on the Determination of the Average Cluster Size*

As previously explained, part of the Rh appeared to be covered with Pt in mixed Pt/Rh clusters. To a lesser extent Pt will be covered with Rh. The amount of Rh on the surface of the Pt/Rh/CeO_2/γ-Al_2O_3 catalyst remains below the LEIS detection limit (Fig. 4). However, to enable determination of the average diameter of the Pt/Rh clusters, the Rh coverage must be added to the visible Pt fraction in the three-way catalyst. Therefore, the surface composition will be calculated using bulk values and thermodynamics.

The final treatment of the Pt/Rh/CeO_2/γ-Al_2O_3 catalyst before LEIS analysis is a 10-min reduction at 573 K. Assuming that the surface composition after this treatment is equal to the equilibrium composition at this temperature in vacuum, the following Pt : Rh ratio can be expected for the bulk $Pt_{0.725}Rh_{0.275}$ three-way catalyst:

$$\left(\frac{X_{Pt}}{X_{Rh}}\right)_{surface} = \left(\frac{X_{Pt}}{X_{Rh}}\right)_{bulk} \times \exp\left(\frac{-\Delta G}{R \times T}\right). \qquad [5]$$

A segregation energy (ΔG) of -6 kJ/mol has been determined experimentally for single crystalline (410) $Pt_{0.25}Rh_{0.75}$ after annealing in vacuum at 573 K (15). Using this value, a $(Pt:Rh)_{surface}$ ratio of 9.28 is found for the bulk $Pt_{0.725}Rh_{0.275}$ three-way catalyst. This ratio corresponds to $Pt_{0.903}Rh_{0.097}$; i.e., 9.7% of the cluster surface area consists of Rh. If this amount is added to the observed Pt ($\vartheta_{Pt} = (1.0 \pm 0.1) \times 10^{-3}$ ML), the noble metal surface coverage of the Pt/Rh/CeO_2/γ-Al_2O_3 catalyst corresponds to $\vartheta = (1.1 \pm 0.1) \times 10^{-3}$ ML. As has been shown for the Pt/γ-Al_2O_3 catalyst, the average cluster diameter can be determined using ϑ. Using $\rho_{Rh} = 12.41 \times 10^6$ g/m^3 (19) and the noble metal weight fractions and BET specific surface area as summarized in Table 1, the average cluster diameter of the Pt/Rh clusters in the Pt/Rh/CeO_2/Al_2O_3 three-way catalyst is 2.7 nm.

One should note that there can be less segregation in very small clusters than in bulk samples (29, 30). To investigate whether the segregation is limited in the three-way catalysts, the noble metal dispersion (D), i.e., the ratio of the surface atoms and the total number of atoms, must be determined. The interatomic distance in $Pt_{0.725}Rh_{0.275}$ is 0.28 nm (31); hence the average cluster diameter of 2.7 nm corresponds to approximately 385 atoms per cluster. When approximating the spherically shaped clusters with a truncated hexagonal bipyramid composed of 377 atoms, 210 of these atoms will be exposed to the surface (32). Hence, the dispersion of the clusters is $D = 0.56$.

Due to the limited number of atoms in the cluster, 56% of the atoms in the noble metal clusters are exposed to the surface, and the segregation of one species leads to a depletion of that species in the bulk of the cluster, which has been neglected in Eq. [5]. To enable correction for the depletion of the bulk we use the relation between the surface and bulk composition,

$$D \times (X_i)_{surface} + (1 - D) \times (X_i)_{bulk} = X_i, \qquad [6]$$

where X_i is the overall fraction of element in the cluster (for the Pt/Rh/CeO_2/Al_2O_3 three-way catalyst clusters $X_{Pt} = 0.725$ and $X_{Rh} = 0.275$). Combining Eqs. [5] and [6] gives $Pt_{0.834}Rh_{0.166}$ for the surface composition and $Pt_{0.588}Rh_{0.412}$ for the bulk composition of the Pt/Rh/CeO_2/Al_2O_3 three-way catalyst clusters. Note that the bulk composition found is significantly different from the overall cluster composition (i.e., $Pt_{0.725}Rh_{0.275}$).

The presence of step edges, however, will increase the Pt surface enrichment. The surface enrichment has been calculated for Pt surface atoms that are missing 4 neighbors. However, at step edges the Pt atoms are missing up to 6 neighbors. Measurements of Moest *et al.* (15) have shown the validity of the broken bond model in explaining the segregation behavior of Pt/Rh. Therefore, ΔG is taken to be directly proportional to the number of missing neighbors.

Van Hardeveld and Hartog (32) report 18 atoms missing 7 neighbors, 42 atoms missing 6 neighbors, 60 atoms

missing 5 neighbors, 6 atoms missing 4 neighbors, 12 atoms missing 3 neighbors, and 72 atoms missing 2 neighbors in a 377-atoms-sized truncated hexagonal bipyramid. (More spherical clusters give similar results.) Using these numbers, correction for the enhanced segregation at step edges gives for the $Pt_{0.725}Rh_{0.275}$ a surface composition of $Pt_{0.866}Rh_{0.134}$.

Since the formation of RhO_2 is thermodynamically more favorable than that of PtO_2 (19), the metal support interaction will further deplete the surface in Rh and enhance Pt segregation. Therefore, the obtained $Pt_{0.866}Rh_{0.134}$ might still be an overestimation of the actual Rh surface percentage. If the cluster–support interface is assumed to consist entirely of Rh oxide, due to the more favorable metal–support interaction, segregation would yield a $Pt_{0.909}Rh_{0.091}$ cluster surface. The $Pt_{0.909}Rh_{0.091}$ corresponds to a Rh depletion of $91/275 = 0.33$, which is in agreement with the experimentally determined value, which equals 0.31 ± 0.02. Using $Pt_{0.909}Rh_{0.091}$ for the surface concentration, Eq. [4] still gives $d = 2.7$ nm for the average cluster diameter of the $Pt/Rh/CeO_2/Al_2O_3$ three-way catalyst. Hence, the agreement found between the experimentally and the thermodynamically determined Rh depletion indicates once more the validity of the average noble metal cluster size as determined with LEIS.

3.6. General Applicability of LEIS to Determine the Size of Clusters with Different Shapes

In this study the cluster sizes of two reduced clusters with contact angles $\alpha = 115°$ have been determined. The method presented can also be used to determine the size of clusters with other contact angles. Even the size of hemispherically shaped clusters ($\alpha = 90°$), which are encountered in oxidized clusters (20, 24), can be determined. Therefore, Fig. 3 gives c_θ as a function of α and, as explained in (24), the visible fraction ϑ does not change for $90° \leq \alpha \leq 180°$. Hence the method can be used for all kinds of pseudospherically shaped clusters.

4. CONCLUSIONS

A method for determining the average cluster size of supported catalysts using LEIS data has been presented. For $Pt/\gamma\text{-}Al_2O_3$, agreement between the average cluster sizes determined with this method and that determined with TEM has been shown. LEIS has been successfully applied to determine the average noble metal cluster size of a ceria-supported commercial three-way catalyst. The average noble metal cluster size of the commercial three-way catalyst is 2.7 nm.

LEIS analysis of $Pt/Rh/\gamma\text{-}Al_2O_3$ and $Rh/\gamma\text{-}Al_2O_3$ showed a Rh surface depletion with a factor of 0.31 ± 0.02 on $Pt/Rh/\gamma\text{-}Al_2O_3$ after reduction at 573 K. This is in agreement with thermodynamic calculations yielding a factor of 0.33 when assuming 2.7-nm clusters that are reduced at 573 K. Hence, the presence of a significant number of pure Rh clusters on the similarly prepared $Pt/Rh/CeO_2/\gamma\text{-}Al_2O_3$ catalyst is very unlikely. The $Pt/Rh/CeO_2/\gamma\text{-}Al_2O_3$ catalyst therefore contains mixed Pt/Rh clusters that are strongly enriched in Pt after reduction. Since the average cluster size as determined with LEIS has been used for the thermodynamical calculations, the agreement found with the experimentally determined Rh depletion provides an additional indication of the validity of the determined cluster size.

The high sensitivity of LEIS for metals permits cluster size determination down to metal loadings of some 10 ppm in the outermost atomic layer of the surface. Moreover, the accuracy of LEIS increases with increasing dispersion, since LEIS selectively detects atoms in the outermost atomic layer. Hence, very small clusters can be determined with the highest possible accuracy, whereas microscopic methods require a minimum cluster size. Moreover, the average cluster size determined with LEIS reflects a statistical average over several square millimeters of catalyst, whereas microscopic techniques probe only minute areas.

ACKNOWLEDGMENTS

Financial support for this study was provided by the Dutch Technology Foundation (STW). The authors are grateful to d**mc**^{2} A. G. (Hanau, Germany) for providing the catalysts. Dr. P. J. Kooyman of the National Centre for High-Resolution Electron Microscopy (Delft, The Netherlands) is gratefully acknowledged for performing the electron microscopy investigations.

REFERENCES

1. Balenovic, M., Backx, A. C. P. M., and Hoebink, J. H. B. J., SAE-Paper 2001-01-0937.
2. Hoebink, J. H. B. J., Harmsen, J. M. A., Balenovic, M., Backx, A. C. P. M., and Schouten, J. C., *Topics Catal.* **16/17**, 397 (2001).
3. Rogemond, E., Essayem, N., Frety, R., Perrichon, V., Primet, M., Chevrier, M., Gauthier, C., and Mathis, F., *J. Catal.* **186**(2), 414 (1999).
4. Holles, J. H., Switzer, M. A., and Davis, R. J., *J. Catal.* **190**(2), 247 (2000).
5. Maunula, T., Ahola, J., Salmi, T., Heikki, H., Härkönen, M., Luoma, M., and Pohjola, V. J., *Appl. Catal. B* **12**, 287 (1997).
6. Holmgren, A., Andersson, B., and Duprez, D., *Appl. Catal. B* **22**(3), 215 (1999).
7. Kip, B. J., Duivenvoorden, F. B. M., Koningsberger, D. C., and Prins, R., *J. Catal.* **105**, 26 (1987).
8. Winkelmann, F., Wohlrab, S., Libuda, J., Bäumer, M., Cappus, D., Menges, M., Al-Shamery, K., Kuhlenbeck, H., and Freund, H.-J., *Surf. Sci.* **307–309**, 1148 (1994).
9. Klimenkov, M., Nepijko, S., Kuhlenbeck, H., Bäumer, M., Schlögl, R., and Freund, H.-J., *Surf. Sci.* **391**, 27 (1997).
10. Fajardie, F., Tempere, J.-F., Manoli, J.-M., Touret, O., and Djéga-Mariadassou, G., *Catal. Lett.* **54**, 187 (1998).
11. Jansen, W. P. A., Knoester, A., Maas, A. J. H., Schmit, P., Denier v.d. Gon, A. W., and Brongersma, H. H., to be published.
12. Harmsen, J. M. A., Jansen, W. P. A., Hoebink, J. H. B. J., Schouten, J. C., and Brongersma, H. H., *Catal. Lett.* **74**, 133 (2001).
13. Bergmans, R., Ph.D. thesis. Eindhoven University of Technology, The Netherlands, 1996.

14. Beck, D. D., DiMaggio, C. L., and Fisher, G. B., *Surf. Sci.* **297**, 293 (1993).
15. Moest, B., Wouda, P. T., Denier v.d. Gon, A. W., Langelaar, M. C., Brongersma, H. H., Nieuwenhuys, B. E., and Boerma, D. O., *Surf. Sci.* **473**, 159 (2001).
16. Den Otter, W. K., Brongersma, H. H., and Feil, H., *Surf. Sci.* **306**, 215 (1994).
17. Ackermans, P. A. J., van der Meulen, P. F. H. M., Ottevanger, H., van Straten, F. E., and Brongersma, H. H., *Nucl. Instr. and Meth. B* **35**, 541 (1988).
18. Campman, M., Ph.D. thesis. Eindhoven University of Technology, The Netherlands, 1996.
19. Lide, D. R., (Ed.), "Handbook of Chemistry and Physics," p. 4–21. CRC Press, Boca Raton, FL, 1995.
20. Diebold, U., Pan, J.-M., and Madey, T. E., *Surf. Sci.* **331–333**, 845 (1994).
21. Clausen, B. S., Schiøtz, J., Gråbæk, L., Ovessen, C. V., Jacobsen, K. W., Nørskov, J. K., and Topsøe, H., *Topics Catal.* **1**, 367 (1994).
22. Tomsia, A. P., and Glaesar, A. M., (Eds.), "Wetting and Work of Adhesion in Oxide-Metal Systems, Ceramic Microstructures, Control at the Atomic Level," p. 65. Plenum, New York, 1998.
23. Bernal, S., Calvino, J. J., Cauqui, M. A., Gatica, J. M., Larese, C., Péreze Omil, J. A., and Pintado, J. M., *Catal. Today* **50**, 175 (1999).
24. V.d. Oetelaar, L. C. A., Partridge, A., Stapel, P. J. A., Flipse, C. F. J., and Brongersma, H. H., *J. Phys. Chem. B* **102**, 9532 (1998).
25. Cortenraad, R., Ermolov, S. N., Moest, B., Denier van der Gon, A. W., Glebovsky, V. G., and Brongersma, H. H., *Nucl. Instr. and Meth. B* **174**, 173 (2001).
26. Kim, S., and D'Aniello, Jr., M. J., *Appl. Catal.* **56**, 23 (1989).
27. Jacobs, J.-P., Lindfors, L. P., Reintjes, J. G. H., Jylhä O., and Brongersma, H. H., *Catal. Lett.* **25**, 315 (1994).
28. Beck, D. D., DiMaggio, C. L., and Fisher G. B., *Surf. Sci.* **297**, 303 (1993).
29. Williams, F. L., and Nason, D., *Surf. Sci.* **45**, 377 (1974).
30. V.d. Oetelaar, L. C. A., Nooij, O. W., Oerlemans, S., Denier v.d. Gon, A. W., and Brongersma, H. H., *J. Phys. Chem. B* **102**, 3445 (1998).
31. Erich Pietsch, E. H., (Ed.), "Gmelin Handbuch der Anorganischen Chemie," Pt teil A p. 831, Springer-Verlag, Berlin, 1951.
32. Van Hardeveld, R., and Hartog, F., *Surf. Sci.* **15**, 189 (1969).